

Duality TV-L1 Flow with Fundamental Matrix Prior

A. Wedel^{1,2}, T. Pock², J. Braun³, U. Franke¹, and D. Cremers²

¹Daimler Group Research, Sindelfingen, Germany.

²Computer Vision Group, University of Bonn, Germany.

³Institute for Numerical Simulation, University of Bonn, Germany.

Email: andreas.wedel@daimler.com

Abstract

Variational techniques yield the most accurate results for dense optical flow fields between two images. They have the nice property of inherent smoothness to cope with untextured image regions: the filling-in of such regions is driven by neighbouring pixels. Such filling-in is not always the best choice. If the scene is mostly stationary and the camera is moving, the direction of the optical flow vectors can be restricted using the fundamental matrix. In this paper we propose an exact solution of the variational optical flow, using the fundamental matrix geometry as an additional weak prior. Our novel approach currently performs best on the Middlebury flow evaluation which includes images from stationary and dynamic scenes.

Keywords: Optical flow, fundamental matrix, structure from motion, optimization, total variation

1 Introduction

Understanding the dynamic movement of a scene is a key component of environment perception. The process of understanding dynamic movements includes the visual perception of motion and the ability to reconstruct the three dimensional scene in a human brain (visual kinesthesia). The perception of motion hence is a preliminary step to reconstruct dynamic scenes. In machine vision, the motion (here: *displacement*) of pixels between two successive images of a sequence is called optical flow.

In the literature local and global approaches are known to estimate the optical flow field. Local feature based approaches analyze a local neighborhood of a pixel and try to find the same pixel neighborhood in a successive frame. This is done differentially (e.g. [1]) or directly by comparing pixel descriptors (e.g. [2]). Feature based approaches have the ability to match large flow vectors, with the drawback of noisy results, especially if the local neighborhood of a pixel is not distinct (low texture). The over-all accuracy is hence worse than the accuracy of global approaches, especially if displacement vectors are small and the flow field is smooth. Global approaches, such as variational optical flow [3, 4, 5] overcome the problem of low texture by introducing a smoothness term, favouring (piecewise) smooth flow fields. However, such smoothing leads to filling-in effects in untextured regions and is not always the best choice.

If prior knowledge, such as the movement of the camera, is known it is favourable to include this knowledge in the estimation process of the optical flow. In robotics such a procedure is well-known in structure from motion based approaches, where the knowledge of the fundamental matrix is explicitly used for feature tracking and detection of moving objects [6, 7]. Variational optical flow techniques with prior knowledge of the fundamental matrix geometry were presented using hard constraints [8] and soft constraints [9], the latter estimating simultaneously the optical flow and the fundamental matrix. The algebraic distance to the epipolar rays was used in both approaches. In this paper we propose a soft constraint using the geometric distance to the fundamental lines, yielding less errors in dynamic scenes.

Our novel approach uses a dual formulation of the total variation optical flow, introduced by [5]. Total variation has the property of piecewise smoothness of the flow field. We include the fundamental matrix prior as an additional data term and present an efficient thresholding scheme for minimizing the data deviation terms. This replaces the commonly used lagged diffusivity approach for multiple data terms. The presented algorithm outperforms all known gray value based optical flow algorithms in all categories on the Middlebury evaluation data set [10] at the time of submission. Our fundamental prior implementation (based on gray values) also performs best on average when compared to all approaches, including those using color.

2 Background

2.1 Variational Optical Flow

Optical flow in a variational framework was first proposed by Horn and Schunck in [3]. Since then, many improvements have been made to incorporate robust illumination (gray value constancy) terms and robust smoothness terms. In this context, robustness denotes a linear instead of a quadratic penalty for both the smoothness and data terms. A nice summary is given in [4].

Variational methods are known to be computationally very complex and real-time performance was first achieved in [11] for small image sizes. Lately [5] presented a real-time total variation optical flow approach using the GPU. The main contribution of [5] is the reformulation of the original variational energy functional into a convex dual form, allowing splitting between the data term and the smoothness term in an iterative solving process.

We take this convex dual formulation of the variational energy functional for optical flow and add a second penalty term. With the primal and dual optical flow vectors $\mathbf{u}(\mathbf{x}) = (u_1(\mathbf{x}), u_2(\mathbf{x}))^\top$ and $\mathbf{v}(\mathbf{x}) = (v_1(\mathbf{x}), v_2(\mathbf{x}))^\top$, for a pixel \mathbf{x} in the image region Ω , the variational energy to be minimized reads $E_\theta(\mathbf{u}, \mathbf{v}) =$

$$\int_{\Omega} |\nabla u_1| + |\nabla u_2| + \frac{\|\mathbf{u} - \mathbf{v}\|^2}{2\theta} + \sum_{i=1}^2 \lambda_i |p_i(\mathbf{v})| dx. \quad (1)$$

The (small) constant θ penalizes deviations between primal and dual flow vectors and the λ_i weight the influence of the penalty terms p_1 and p_2 , respectively. In the above energy functional, p_1 and p_2 encode the common gray value constancy term (see for example [5, 4])

$$p_1(\mathbf{v}) = I(t) - I(t-1) + \mathbf{v}^\top \nabla I(t) \quad (2)$$

and the fundamental matrix deviation term

$$p_2(\mathbf{v}) = \gamma(\tilde{\mathbf{x}} + \tilde{\mathbf{v}})^\top F \tilde{\mathbf{x}} = \gamma \tilde{\mathbf{x}}^\top F \tilde{\mathbf{x}} + \gamma \tilde{\mathbf{v}}^\top F \tilde{\mathbf{x}}. \quad (3)$$

In the fundamental matrix deviation term, tilted variables are homogeneous extensions of the variable, i.e. $\tilde{\mathbf{x}}^\top = [\mathbf{x}^\top, 1]$ and $\tilde{\mathbf{v}}^\top = [\mathbf{v}^\top, 0]$. F represents the 3×3 fundamental matrix. The factor γ is used to approximate the geometric distance to the epipolar rays computed from F (using the Sampson error, a first order approximation). According to [12] it is computed as

$$\gamma^{-1} = \sqrt{(\tilde{\mathbf{x}}_v^\top F)_1^2 + (\tilde{\mathbf{x}}_v^\top F)_2^2 + (F \tilde{\mathbf{x}})_1^2 + (F \tilde{\mathbf{x}})_2^2} \quad (4)$$

where sub-indexes indicate first and second entries of the vectors respectively and $\tilde{\mathbf{x}}_v = \tilde{\mathbf{x}} + \tilde{\mathbf{v}}$. The factor γ is calculated using flow vectors of the last iteration (hence we use lagged feedback for computing the scale factor γ).

2.2 Minimizing the Energy

For fixed θ and λ_i , the energy (Equation (1)) is minimized by alternating the two steps of updating \mathbf{u} and \mathbf{v} until convergence.

(1) Smoothness: For every v_d being fixed, solve

$$\min_{u_d} \int_{\Omega} \left\{ |\nabla u_d| + \frac{1}{2\theta} (u_d - v_d)^2 \right\} dx. \quad (5)$$

This is the image denoising model introduced in [13]. An efficient algorithm is based on gradient descent and subsequent re-projection using the dual-ROF model [14]. The solution computes as

$$u_d = v_d + \theta \mathbf{div} \mathbf{p}, \quad (6)$$

where $\mathbf{p} = [p_1, p_2]$ is defined iteratively by

$$\tilde{\mathbf{p}}^{n+1} = \mathbf{p} + \frac{\tau}{\theta} (\nabla (f + \lambda \mathbf{div} \mathbf{p}^n)) \quad (7)$$

$$\mathbf{p}^{n+1} = \frac{\tilde{\mathbf{p}}^{n+1}}{\max\{1, |\tilde{\mathbf{p}}^{n+1}|\}}. \quad (8)$$

(2) Data: In a second step, for \mathbf{u} being fixed, solve

$$\min_{\mathbf{v}} \left\{ \frac{1}{2\theta} \|\mathbf{u} - \mathbf{v}\|^2 + \lambda_1 |p_1(\mathbf{v})| + \lambda_2 |p_2(\mathbf{v})| \right\}. \quad (9)$$

Note, that we have dropped the integral sign. The solution only depends on the variable $\mathbf{v}(x)$ and no spatial terms contribute. This simplifies the solution scheme: a local (pixel wise) solution for every image pixel yields the global optimal minimum for this second step.

2.3 Quadratic Optimization

Equation (9) is a combination of convex functions, and hence is convex itself. The minimum is unique, unless both data terms and the flow vector \mathbf{u} are equal to zero. If (9) would be differentiable, the minimum could be found by setting its derivative, with respect to \mathbf{v} , equal to zero.

However, the absolute function $|p_i|$ is degenerate at $|p_i| = 0$ and not differentiable. More sophisticated quadratic optimization techniques have to be used to find the minimum of (9). In this subsection, we rewrite the optimization problem with the absolute function into a quadratic optimization problem with inequality constraints. Also, the basics for optimization techniques based on quadratic optimization are presented. Section 3 then presents a fast and optimal thresholding scheme for solving the resulting quadratic optimization problem in the data terms.

First, we rewrite (9) to get a simpler notation. Because θ and λ_i are both positive, we can multiply (9) with θ and place λ_i into the data penalty terms p_i yielding

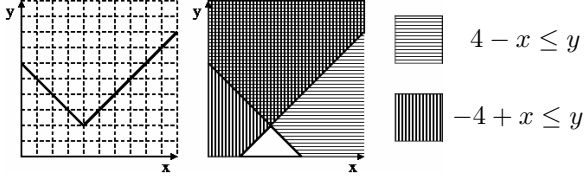


Figure 1: Example for finding $\min_x \{2 + |4 - x|\}$ (minimum $x^* = 4$). The $|\cdot|$ function is replaced by a dual variable y and inequality constraints (*equations to right of graph*), yielding $\min_{x,y} \{2 + y\}$. The new minimum is $(x^*, y^*) = (4, 2)$. Note that both problems yield the same minimum for the primal variable x^* .

$$\min_{\mathbf{v}} \left\{ \frac{1}{2} \|\mathbf{u} - \mathbf{v}\|^2 + |\theta \lambda_1 p_1(\mathbf{v})| + |\theta \lambda_2 p_2(\mathbf{v})| \right\}.$$

A closer look at the penalty functions p_1 and p_2 reveals that both are linear in \mathbf{v} . Therefore, there exist constants a_i and b_i , such that:

$$\begin{aligned} \theta \lambda_1 p_1(\mathbf{v}) &= a_0 + a_1 v_1 + a_2 v_2 = a_0 + \mathbf{a}^\top \mathbf{v}, \\ \theta \lambda_2 p_2(\mathbf{v}) &= b_0 + b_1 v_1 + b_2 v_2 = b_0 + \mathbf{b}^\top \mathbf{v}. \end{aligned} \quad (10)$$

In a next step, the absolute functions are replaced by a dual variables y_a , y_b and inequality constraints (see figure 1 for an example). The remaining minimization problem is to find the minimum of

$$\frac{1}{2} (u_1 - v_1)^2 + (u_2 - v_2)^2 + y_a + y_b \quad (11)$$

with the four inequality constraints

$$\begin{aligned} \text{(a)} \quad & a_0 + \mathbf{a}^\top \mathbf{v} - y_a \leq 0, \\ \text{(b)} \quad & -a_0 - \mathbf{a}^\top \mathbf{v} - y_a \leq 0, \\ \text{(c)} \quad & b_0 + \mathbf{b}^\top \mathbf{v} - y_b \leq 0, \text{ and} \\ \text{(d)} \quad & -b_0 - \mathbf{b}^\top \mathbf{v} - y_b \leq 0. \end{aligned} \quad (12)$$

(11) under the side condition (12) yields the same minimum as (9). We replaced the absolute function and have a differentiable objective function. This however is at the cost of two additional variables and four inequality constraints. We present a simple solution by looking at all possible restrictions of the p_i , namely $p_i \leq 0$, $p_i \geq 0$, and $p_i = 0$ in Section 3. The fulfillment of the sufficient and necessary conditions of a global minimum will be proved using the above derived dual formulation of the problem:

For a quadratic minimization problem $\min_x \{f(x)\}$, under linear inequality constraints $g_i(x) \leq 0$, a global optimum of a solution x^* holds true if there exist constants μ_i such that the Karush-Kuhn-Tucker (KKT) conditions [15] are fulfilled:

$$\text{Stationarity: } \nabla f(x^*) + \sum_i \mu_i \nabla g_i(x^*) = 0.$$

$$\text{Primal feasibility: } g_i(x^*) \leq 0.$$

$$\text{Dual feasibility: } \mu_i \geq 0.$$

$$\text{Complementary slackness: } \mu_i g_i(x) = 0 \quad \forall i.$$

2.4 Warping and Fundamental Matrix

We employ a pyramid and warping scheme for the optical flow, as proposed in [4, 5] to estimate large flow vectors. In every warping iteration, the functional (1) is minimized iteratively subject to the variables \mathbf{u} and \mathbf{v} for a certain number of iterations (10 iterations in our experiments). Solving for \mathbf{u} , an inner iteration loop is required. In the experiments we set the number of warps per pyramid level to 15 and the number of inner loops to 1. For real-time applications these settings should be reversed.

The fundamental matrix parameters, denoted as F , are either given to the algorithm or computed online. For many applications, such as driver assistance, the movement of the camera is either known or an accurate initial guess is available. In the Middlebury data set neither the camera motion nor the camera intrinsic are known and the fundamental matrix has to be estimated online. We start with the zero (empty) matrix and solve for the matrix parameters by minimizing the geometric distance in each image warp on both uppermost image pyramid levels (highest resolution). We use an iteratively re-weighted least squares method, as proposed in [12].

3 Data Term Thresholding

In this section we propose and verify an efficient solution scheme to minimize the objective function (9) or, equivalently, its dual quadratic optimization problem (11) with inequality constraints (12).

Looking at all possible combinations of the data terms $|p_i|$, namely $p_i \leq 0$, $p_i \geq 0$, and $p_i = 0$, directly yields a thresholding scheme to minimize the objective function. If both p_1 and p_2 are strictly positive or negative ($p_i \neq 0$), the optimal solution \mathbf{v}^* is found iff the following checks apply:

Assume $p_{1,2}(\mathbf{v}^*)$	Thresholding Checks	Solution $\mathbf{v}^* =$
$p_1 \geq 0$ $p_2 \geq 0$	$a_0 + \mathbf{a}^\top (\mathbf{u} - \mathbf{a} - \mathbf{b}) \geq 0$ $b_0 + \mathbf{b}^\top (\mathbf{u} - \mathbf{a} - \mathbf{b}) \geq 0$	$\mathbf{u} - \mathbf{a} - \mathbf{b}$
$p_1 \geq 0$ $p_2 \leq 0$	$a_0 + \mathbf{a}^\top (\mathbf{u} - \mathbf{a} + \mathbf{b}) \geq 0$ $b_0 + \mathbf{b}^\top (\mathbf{u} - \mathbf{a} + \mathbf{b}) \leq 0$	$\mathbf{u} - \mathbf{a} + \mathbf{b}$
$p_1 \leq 0$ $p_2 \geq 0$	$a_0 + \mathbf{a}^\top (\mathbf{u} + \mathbf{a} - \mathbf{b}) \leq 0$ $b_0 + \mathbf{b}^\top (\mathbf{u} + \mathbf{a} - \mathbf{b}) \geq 0$	$\mathbf{u} + \mathbf{a} - \mathbf{b}$
$p_1 \leq 0$ $p_2 \leq 0$	$a_0 + \mathbf{a}^\top (\mathbf{u} + \mathbf{a} + \mathbf{b}) \leq 0$ $b_0 + \mathbf{b}^\top (\mathbf{u} + \mathbf{a} + \mathbf{b}) \leq 0$	$\mathbf{u} + \mathbf{a} + \mathbf{b}$

Table 1: Minimum \mathbf{v}^* if $p_1(\mathbf{v}^*) \neq 0$ and $p_2(\mathbf{v}^*) \neq 0$

Proof: For $p_1 \neq 0$ and $p_2 \neq 0$ the solution can be found by setting the derivative of the unconstrained objective function equal to zero. We will

prove using the KKT conditions, that this yields a global minimum iff the above thresholding steps succeed. Due to construction, exactly two inequality constraints for the y_i are binding (the left side is 0). We set the μ_i for these constraints to 1 and the μ_i for the other two constraints to 0. This implies that the point is stationary because the solution is constructed to yield a derivative of zero. It directly follows, that complementary slackness and dual feasibility hold. The thresholding check ensures primal feasibility of the solution and hence, iff the thresholding check succeeds, a global minimal solution is found.

3.1 Vanishing data terms

If (at least) one of the data terms is binding, the solution space is restricted to yield either $p_1(\mathbf{v}^*) = 0$ or $p_2(\mathbf{v}^*) = 0$. In this subsection we derive thresholding checks to verify the necessary and sufficient conditions of a global minimum for the local solution in these restricted cases. For the following analysis, we assume that the first data term at the global minimum vanishes, i.e. $p_1(\mathbf{v}^*) = 0$. The case $p_2(\mathbf{v}^*)$ is equivalent (simply exchange the two data terms) and not handled explicitly.

For a vanishing p_1 , three cases need to be examined: $p_2(\mathbf{v}^*) < 0$, $p_2(\mathbf{v}^*) = 0$, and $p_2(\mathbf{v}^*) > 0$. The case $p_2(\mathbf{v}^*) = 0$ is left out in the analysis. If all other cases do not yield a global minimum, it directly follows that both data terms must vanish; the unknown parameter vector v can then be calculated from the two data term equations.

For now we stick with $p_1(\mathbf{v}^*) = 0$ and assume either $p_2(\mathbf{v}^*) > 0$ or $p_2(\mathbf{v}^*) < 0$. The (possible) global minimum \mathbf{v}^* is computed by setting the derivative of the objective function (9) equal to zero using the assumptions made on the p_i :

Assume	Solution
$p_1(\mathbf{v}^*) = 0$	(checks follow)
$p_2(\mathbf{v}^*) \geq 0$	$\mathbf{v}^* = \mathbf{u} - \mathbf{b} - \frac{\mathbf{a}}{\mathbf{a}^\top \mathbf{a}} (a_0 + \mathbf{a}^\top \mathbf{u} - \mathbf{a}^\top \mathbf{b})$
$p_2(\mathbf{v}^*) \leq 0$	$\mathbf{v}^* = \mathbf{u} + \mathbf{b} - \frac{\mathbf{a}}{\mathbf{a}^\top \mathbf{a}} (a_0 + \mathbf{a}^\top \mathbf{u} + \mathbf{a}^\top \mathbf{b})$

Table 2: Minimum \mathbf{v}^* if $p_1(\mathbf{v}^*) = 0$ and $p_2(\mathbf{v}^*) \neq 0$.

Again, we have to check the KKT conditions to verify a global optimum. Due to construction we have $y_a = 0$, and the first two inequality constraints are binding (hence primal feasible). Out of the remaining two inequality constraints, one is primal feasible due to construction as $p_2(\mathbf{v}^*) \leq 0$ or $p_2(\mathbf{v}^*) \geq 0$ directly yields that one inequality constraint is binding. The last constraint is checked by the thresholding step in table 3.

The complementary slackness condition states that the μ_i corresponding to the only non-binding in-

First thresholding check if $p_1(\mathbf{v}^*) = 0$
for $p_2(\mathbf{v}^*) \geq 0$ check
$b_0 + \mathbf{b}^\top (\mathbf{u} - \mathbf{b} - \frac{\mathbf{a}}{\mathbf{a}^\top \mathbf{a}} (a_0 + \mathbf{a}^\top \mathbf{u} - \mathbf{a}^\top \mathbf{b})) \geq 0,$
for $p_2(\mathbf{v}^*) \leq 0$ check
$b_0 + \mathbf{b}^\top (\mathbf{u} + \mathbf{b} - \frac{\mathbf{a}}{\mathbf{a}^\top \mathbf{a}} (a_0 + \mathbf{a}^\top \mathbf{u} + \mathbf{a}^\top \mathbf{b})) \leq 0.$

Table 3: Check for primal feasibility.

equality constraint has to be zero. This leaves us with three more μ_i , which have to be positive to fulfill the dual feasibility condition.

Example: Let us assume, $p_2(\mathbf{v}^*) \geq 0$. It follows that the inequality constraint (12.c) is binding and the inequality constraint (12.d) is fulfilled. This directly implies that μ_d has to be zero (as stated above).

Using the KKT stationarity condition, we derive an equation system to solve for the remaining μ_i :

$$\begin{bmatrix} a_1 & -a_1 & b_1 \\ a_2 & -a_2 & b_2 \\ -1 & -1 & 0 \\ 0 & 0 & -1 \end{bmatrix} \begin{bmatrix} \mu_a \\ \mu_b \\ \mu_c \end{bmatrix} = \begin{bmatrix} u_1 - v_1 \\ u_2 - v_2 \\ -1 \\ -1 \end{bmatrix}$$

From this it follows that $\mu_c = 1$ and the remaining system of equations yields a unique solution for μ_a and μ_b . This can be seen when plugging back in the possible solutions for \mathbf{v}^* , yielding:

$$\begin{aligned} a_1(\mu_a - \mu_b) &= \frac{a_1}{\mathbf{a}^\top \mathbf{a}} (a_0 + \mathbf{a}^\top \mathbf{u} - \mathbf{a}^\top \mathbf{b}) \\ a_2(\mu_a - \mu_b) &= \frac{a_2}{\mathbf{a}^\top \mathbf{a}} (a_0 + \mathbf{a}^\top \mathbf{u} - \mathbf{a}^\top \mathbf{b}) \\ \mu_a + \mu_b &= 1 \end{aligned}$$

The solution is given by

$$\mu_a = \frac{1}{2\mathbf{a}^\top \mathbf{a}} (a_0 + \mathbf{a}^\top \mathbf{u} - \mathbf{a}^\top \mathbf{b}) + \frac{1}{2} \quad (13)$$

$$\mu_b = \frac{-1}{2\mathbf{a}^\top \mathbf{a}} (a_0 + \mathbf{a}^\top \mathbf{u} - \mathbf{a}^\top \mathbf{b}) + \frac{1}{2}. \quad (14)$$

The KKT dual feasibility constraint states that both, μ_a and μ_b have to be positive. This can be checked very efficiently:

Second thresholding check if $p_1(\mathbf{v}^*) = 0$
check $\left \frac{1}{\mathbf{a}^\top \mathbf{a}} (a_0 + \mathbf{a}^\top \mathbf{u} - \mathbf{a}^\top \mathbf{b}) \right \leq 1$ if $p_2(\mathbf{v}^*) \geq 0$
check $\left \frac{1}{\mathbf{a}^\top \mathbf{a}} (a_0 + \mathbf{a}^\top \mathbf{u} + \mathbf{a}^\top \mathbf{b}) \right \leq 1$ if $p_2(\mathbf{v}^*) \leq 0$

Table 4: Check for dual feasibility.

Iff all KKT conditions hold, \mathbf{v}^* yields a global minimum of the objective function. Following the arguments above, the check for $p_2(\mathbf{v}^*) = 0$ is straightforward. The presented thresholding scheme yields a very efficient and exact total variation scheme for the optical flow with two (linear) data terms.

Average angle error	avg. rank	Army (Hidden texture)			Mequon (Hidden texture)			Schefflera (Hidden texture)			Wooden (Hidden texture)			Grove (Synthetic)			Urban (Synthetic)			Yosemite (Synthetic)			Teddy (Stereo)								
		GT	im0	im1	GT	im0	im1	GT	im0	im1	GT	im0	im1	GT	im0	im1	GT	im0	im1	GT	im0	im1	GT	im0	im1						
		all	disc	untext	all	disc	untext	all	disc	untext	all	disc	untext	all	disc	untext	all	disc	untext	all	disc	untext	all	disc	untext						
F-TV-L1 [18]	4.0	5.44	12.5	5.89	5.46	15.0	4.03	7.48	16.3	3.42	5.08	23.3	2.81	3.42	4.34	3.03	4.05	15.1	3.18	2.43	3.92	1.87	3.90	9.35	2.61						
Fusion [8]	5.5	4.43	13.7	4.08	2.47	8.91	2.24	3.70	9.68	3.12	3.68	19.8	2.54	4.26	5.16	4.31	6.32	16.8	6.15	4.55	14	5.78	14	3.10	7.12	13.6	7.86				
SegOF [12]	5.5	5.85	13.5	3.98	7.40	14.9	8.13	8.55	17.3	9.01	6.50	18.1	5.14	3.95	4.57	4.87	6.67	21.4	10	6.97	1.65	3.49	1.08	3.71	9.23	3.63					
CBF [13]	6.2	3.96	10.2	3.45	3.65	10.3	3.84	5.46	13.4	3.34	3.60	21.5	1.86	4.51	5.57	11	4.00	13.7	14	21.2	15.1	15	6.57	16	7.34	17	10.8	5.23	11.0	5.27	
GraphCuts [16]	7.0	6.25	14.3	5.53	8.60	10	20.1	11	6.61	7.91	15.4	10.9	4.88	5.19	2.00	3.05	6.86	4.78	4.15	9.70	11	15.4	6.83	4.04	12	4.87	4.85	6.35	6	12.2	6.05

Figure 2: Evaluation results on the Middlebury data set [10]. The method proposed in this paper (F-TL-L1) outperforms other approaches by more than one rank on average. Results on stationary scenes, such as *Grove* and *Urban* demonstrate accurate flow estimation and recovery of the fundamental matrix ($\lambda_1 = 45$, $\lambda_2 = 0.22$).



Figure 3: Optical flow for a scene with a running person and a moving camera, installed in a vehicle. Flow above 15px is color-saturated. The distance to the epipolar rays encodes independently moving objects. Clearly, the running person becomes visible ($\lambda_{1,2}$ as in figure 2).

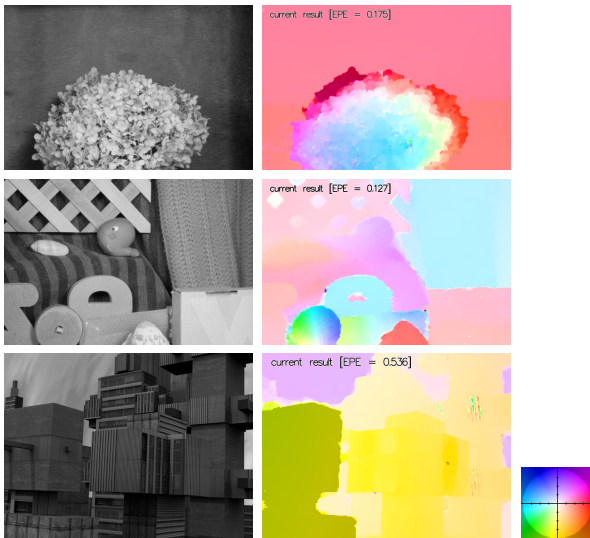


Figure 4: Optical flow results for the *Hydrangea*, *Rubber Whale*, and *Urban3* scene of the Middlebury flow evaluation (color cone shown on the right). Compare with the quantitative results in table 5.

	$\lambda_2 = 0$	$\lambda_2 = 0.22$	$\lambda_2 = 2.25$
Dimetrodon	0.205	0.216	0.356
Grove2	0.154	0.149	0.157
Grove3	0.641	0.626	0.646
Hydrangea	0.158	0.175	0.861
RubberWhale	0.100	0.127	0.371
Urban2	0.346	0.323	0.313
Urban3	0.775	0.725	0.536
Venus	0.262	0.261	0.257

Table 5: Average end point error for the Middlebury scenes with available ground truth ($\lambda_1 = 45$). Optical flow is computed on structure-texture (4 : 1) images (generated using the ROF model with $\lambda = 10$ [16]). Results are median-filtered to discard outliers.

4 Experiments and Results

We evaluated the optical flow algorithm with the fundamental prior on the Middlebury database for optical flow [10]. The evaluation results are shown in figure 2. Out of 16 statistical measurements we perform best in 13 categories. A closer look reveals, that our performance benefits from the fact that 4 out of the 8 test sequences show stationary scenes. Our method is ranked second-place and third-place in the two *standard deviation* categories. This is mainly due to outliers which are more efficiently removed using other approaches.

Figure 4 shows three exemplary flow fields for the Middlebury data set where the ground truth optical flow is known (these are not used for evaluation). The first two examples, *Hydrangea* and *Rubber Whale*, show dynamic scenes while the *Urban3* scene is static. Quantitative results are shown in table 5. While using the fundamental prior slightly worsens the result in dynamic scene, it improves the result in static scenes, as one would expect. However, giving too much influence to the fundamental prior worsens the results in the *Grove* scenes due to the online estimation of the fundamental matrix. If the ground truth fundamental matrix is used, we could not see these effects (although a large λ_2 slows down the convergence).

Figure 3 shows a real world scene with a moving camera. Most of the image, except for the running person, is static and the expanding flow field should follow the epipolar rays. The results show that, except for the Mercedes star and the running person, this assumption holds. While it is not scope of this paper to segment moving objects, the results are well suited to detect independently moving regions

of the image. There are however more constraints than only the *distance to epipolar rays constraint* to detect moving objects (see [7]).

5 Summary and Future Work

In this paper we presented a novel approach to exact variational flow with two data terms. For the first data term we used the commonly known gray value constancy assumption. We used a fundamental matrix prior within the second data term. A direct thresholding scheme was introduced which enables an efficient and exact minimization of the data deviation terms.

The optical flow with the fundamental matrix prior was evaluated on the Middlebury data set for flow evaluation. If compared to *gray value based* algorithms, it performs best in all 16 statistical evaluation category. Algorithms based on *color information* perform better in 3 categories, where we are placed second and third at the time of submission. We expect some minor performance boost when integrating color information in our approach.

An interesting research goal is the integration of local and global features in an optical flow framework. This may imply that the data terms are no longer convex and the optimization scheme may need to be altered.

We are currently investigating three-dimensional scene flow. In the three-dimensional case, priors are even more important to bound the influence of outliers. A very interesting challenge is to use the trifocal tensor within a variational framework for scene-flow estimation from stereo sequences.

References

- [1] B. D. Lucas and T. Kanade, "An iterative image registration technique with an application to stereo vision," in *Proceedings International Joint Conference on Artificial Intelligence*, 1981, pp. 674–679.
- [2] F. Stein, "Efficient computation of optical flow using the census transform," in *Lecture Notes in Computer Science*, Berlin, Germany, 2004, pp. 79–86.
- [3] B. K. Horn and B. G. Schunck, "Determining optical flow," Massachusetts Institute of Technology, Cambridge, USA, Tech. Rep., 1980.
- [4] T. Brox, A. Bruhn, N. Papenberg, and J. Weickert, "High accuracy optical flow estimation based on a theory for warping," in *European Conference on Computer Vision (ECCV)*, vol. 3024, Prague, Czech Republic, May 2004, pp. 25–36.
- [5] C. Zach, T. Pock, and H. Bischof, "A duality based approach for realtime tv-l1 optical flow," in *Pattern Recognition (Proc. DAGM)*, Heidelberg, Germany, 2007, pp. 214–223.
- [6] C. Rabe, C. Volmer, and U. Franke, "Kalman filter based detection of obstacles and lane boundary," in *Autonome Mobile Systems*, vol. 19, 2005, pp. 51–58.
- [7] T. Vaudrey, D. Gruber, A. Wedel, and J. Klappstein, "Space-time multi-resolution banded graph-cut for fast segmentation," in *Pattern Recognition (Proc. DAGM)*, Munich, Germany, June 2008.
- [8] N. Slesareva, A. Bruhn, and J. Weickert, "Optic flow goes stereo: A variational method for estimating discontinuity-preserving dense disparity maps," in *Pattern Recognition (Proc. DAGM)*, Berlin, Germany, 2005, pp. 33–40.
- [9] L. Valgaerts, A. Bruhn, and J. Weickert, "A variational approach for the joint recovery of the optical flow and the fundamental matrix," in *Pattern Recognition (Proc. DAGM)*, Munich, Germany, June 2008.
- [10] S. Baker, S. Roth, D. Scharstein, M. Black, J. Lewis, and R. Szeliski, "A database and evaluation methodology for optical flow," in *International Conference Computer Vision*, 2007, pp. 1–8.
- [11] A. Bruhn, J. Weickert, C. Feddern, T. Kohlberger, and C. Schnörr, "Variational optical flow computation in real time." *IEEE Transactions on Image Processing*, no. 5, pp. 608–615, 2005.
- [12] J. Klappstein, "Optical-flow based detection of moving objects in traffic scenes," Ph.D. dissertation, University of Heidelberg, 2008.
- [13] L. I. Rudin, S. Osher, and E. Fatemi, "Non-linear total variation based noise removal algorithms," *Phys. D*, vol. 60, no. 1-4, pp. 259–268, 1992.
- [14] A. Chambolle, "Total variation minimization and a class of binary MRF models," *Energy Minimization Methods in Computer Vision and Pattern Recognition*, pp. 136–152, 2005.
- [15] W. Karush, "Minima of functions of several variables with inequalities as side constraints," Ph.D. dissertation, Dept. of Mathematics, Univ. of Chicago, 1939.
- [16] J.-F. Aujol, G. Gilboa, T. Chan, and S. Osher, "Structure-texture image decomposition—modeling, algorithms, and parameter selection," *Int. J. Comput. Vision*, vol. 67, no. 1, pp. 111–136, 2006.